Simulations of solid-liquid friction at ice-I_h / water interfaces

Patrick B. Louden and J. Daniel Gezelter*
Department of Chemistry and Biochemistry,
University of Notre Dame
Notre Dame, Indiana 46556

October 23, 2013

Abstract

We have investigated the structural and dynamic properties of the basal and prismatic facets of the ice I_h / water interface when the solid phase is drawn through the liquid (i.e. sheared relative to the fluid phase). To impose the shear, we utilized a velocity-shearing and scaling (VSS) approach to reverse non-equilibrium molecular dynamics (RNEMD). This method can create simultaneous temperature and velocity gradients and allow the measurement of transport properties at interfaces. The interfacial width was found to be independent of the relative velocity of the ice and liquid layers over a wide range of shear rates. Decays of molecular orientational time correlation functions gave similar estimates for the width of the interfaces, although the short- and longer-time decay components behave differently closer to the interface. Although both facets of ice are in "stick" boundary conditions in liquid water, the solid-liquid friction coefficients were found to be significantly different for the basal and prismatic facets of ice.

*Corresponding author. Electronic mail: gezelter@nd.edu

1 Introduction

Understanding the ice/water interface is essential for explaining complex processes such as nucleation and crystal growth,[1–3] crystal melting,[1,4–6] and some fascinating biological processes, such as the behavior of the antifreeze proteins found in winter flounder,[7,8] and certain terrestrial arthropods.[9,10] There has been significant progress on understanding the structure and dynamics of quiescent ice/water interfaces utilizing both theory and experiment. Haymet *et al.* have done extensive work on ice I_h, including characterizing and determining the width of the ice/water interface for the SPC,[11] SPC/E,[12,13] CF1,[14,15] and TIP4P[16] models for water. More recently, Haymet *et al.* have investigated the effects cations and anions have on crystal nucleation.[17–20] Nada *et al.* have also studied ice/water interfaces,[21–24] and have found that the differential growth rates of the facets of ice I_h are due to the the reordering of the hydrogen bonding network.[25]

The movement of liquid water over the facets of ice has been less thoroughly studied than the quiescent surfaces. This process is potentially important in understanding transport of large blocks of ice in water (which has important implications in the earth sciences), as well as the relative motion of crystal-crystal interfaces that have been separated by nanometer-scale fluid domains. In addition to understanding both the structure and thickness of the interfacial regions, it is important to understand the molecular origin of friction, drag, and other changes in dynamical properties of the liquid in the regions close to the surface that are altered by the presence of a shearing of the bulk fluid relative to the solid phase.

In this work, we apply a recently-developed velocity shearing and scaling approach to reverse non-equilibrium molecular dynamics (VSS-RNEMD). This method makes it possible to calculate transport properties like the interfacial thermal conductance across heterogeneous interfaces,[26] and can create simultaneous temperature and velocity gradients and allow the measurement of friction and thermal transport properties at interfaces. This has allowed us to investigate the width of the ice/water interface as the ice is sheared through the liquid, while simultaneously imposing a weak thermal gradient to prevent frictional heating of the interface. In the sections that follow, we discuss the methodology for creating and simulating ice/water interfaces under shear and provide results from both structural and dynamical correlation functions. We also show that the solid-liquid interfacial friction coefficient depends sensitively on the details of the surface morphology.

2 Methodology

2.1 Stable ice I_h / water interfaces under shear

The structure of ice I_h is well understood; it crystallizes in a hexagonal space group $P6_3/mmc$, and the hexagonal crystals of ice have two faces that are commonly exposed, the basal face $\{0\ 0\ 0\ 1\}$, which forms the top and bottom of each hexagonal plate, and the prismatic $\{1\ 0\ \bar{1}\ 0\}$ face which forms the sides of the plate. Other less-common, but still important, faces of ice I_h are the secondary prism, $\{1\ 1\ \bar{2}\ 0\}$, and pyramidal, $\{2\ 0\ \bar{2}\ 1\}$, faces. Ice I_h is normally proton disordered in bulk crystals, although the surfaces probably have a preference for proton ordering along strips of dangling H-atoms and Oxygen lone pairs.[27]

Table 1: Mapping between the Miller indices of four facets of ice in the $P6_3/mmc$ crystal system to the orthorhombic $P2_12_12_1$ system in reference 28.

crystal face	hexagonal ($P6_3/mmc$) Miller indices	orthorhombic ($P2_12_12_1$) equivalent
basal	$\{0\ 0\ 0\ 1\}$	$\{0\ 0\ 1\}$
prism	$\{1\ 0\ \bar{1}\ 0\}$	$\{1\ 0\ 0\}$
secondary prism	$\{1\ 1\ \bar{2}\ 0\}$	$\{1\ 3\ 0\}$
pyramidal	$\{2\ 0\ \bar{2}\ 1\}$	$\{2\ 0\ 1\}$

For small simulated ice interfaces, it is useful to work with proton-ordered, but zero-dipole crystal that exposes these strips of dangling H-atoms and lone pairs. When placing another material in contact with one of the ice crystalline planes, it is also quite useful to have an orthorhombic (rectangular) box. Recent work by Hirsch and Ojamäe describes a number of alternative crystal systems for proton-ordered bulk ice I_h using orthorhombic cells.[28]

In this work, we are using Hirsch and Ojamäe's structure 6 which is an orthorhombic cell ($P2_12_12_1$) that produces a proton-ordered version of ice I_h. Table 1 contains a mapping between the Miller indices of common ice facets in the $P6_3/mmc$ crystal system and those in the Hirsch and Ojamäe $P2_12_12_1$ system.

Structure 6 from the Hirsch and Ojamäe paper has lattice parameters $a = 4.49225$ Å , $b = 7.78080$ Å , $c = 7.33581$ Å and two water molecules whose atoms reside at fractional coordinates

given in table 2. To construct the basal and prismatic interfaces, these crystallographic coordinates were used to construct an orthorhombic unit cell which was then replicated in all three dimensions yielding a proton-ordered block of ice I_h. To expose the desired face, the orthorhombic representation was then cut along the (001) or (100) planes for the basal and prismatic faces respectively. The resulting block was rotated so that the exposed faces were aligned with the z-axis normal to the exposed face. The block was then cut along two perpendicular directions in a way that allowed for perfect periodic replication in the x and y axes, creating a slab with either the basal or prismatic faces exposed along the z axis. The slab was then replicated in the x and y dimensions until a desired sample size was obtained.

Table 2: Fractional coordinates for water in the orthorhombic $P2_12_12_1$ system for ice I_h in reference 28.

atom type	x	y	z
O	0.7500	0.1667	0.4375
H	0.5735	0.2202	0.4836
H	0.7420	0.0517	0.4836
O	0.2500	0.6667	0.4375
H	0.2580	0.6693	0.3071
H	0.4265	0.7255	0.4756

Our ice / water interfaces were created using a box of liquid water that had the same dimensions (in x and y) as the ice block. Although the experimental solid/liquid coexistence temperature under atmospheric pressure is close to 273 K, Haymet *et al.* have done extensive work on characterizing the ice/water interface, and find that the coexistence temperature for simulated water is often quite a bit different.[11,13–16] They have found that for the SPC/E water model,[29] which is also used in this study, the ice/water interface is most stable at 225 $\pm$5 K.[13] This liquid box was therefore equilibrated at 225 K and 1 atm of pressure in the NPAT ensemble (with the z axis allowed to fluctuate to equilibrate to the correct pressure). The liquid and solid systems were combined by carving out any water molecule from the liquid simulation cell that was within 3 Å of any atom in the ice slab. The resulting basal system was $23.87 \times 35.83 \times 98.64$ Å with 900 SPC/E molecules in the ice slab, and 1846 in the liquid phase. Similarly, the prismatic system was $36.12 \times 36.43 \times 86.10$ Å with 1000 SPC/E molecules in the ice slab and 2684 in the liquid.

Molecular translation and orientational restraints were applied in the early stages of equilibration to prevent melting of the ice slab. These restraints were removed during NVT equilibration, well before data collection was carried out.

2.2 Shearing ice / water interfaces without bulk melting

As a solid is dragged through a liquid, there is frictional heating that will act to melt the interface. To study the behavior of the interface under a shear stress without causing the interface to melt, it is necessary to apply a weak thermal gradient in combination with the momentum gradient. This can be accomplished using the velocity shearing and scaling (VSS) variant of reverse non-equilibrium molecular dynamics (RNEMD), which utilizes a series of simultaneous velocity exchanges between two regions within the simulation cell.[26] One of these regions is centered within the ice slab, while the other is centrally located in the liquid region. VSS-RNEMD provides a set of conservation constraints for creating either a momentum flux or a thermal flux (or both simultaneously) between the two slabs. Satisfying the constraint equations ensures that the new configurations are sampled from the same NVE ensemble as before the VSS move.

The VSS moves are applied periodically to scale and shift the particle velocities ($\mathbf{v}_i$ and $\mathbf{v}_j$) in two slabs (H and C) which are separated by half of the simulation box,

$$\begin{array}{rcccc} & \underline{\text{shearing}} & & \underline{\qquad\qquad\text{scaling}\qquad\qquad} & \\ \mathbf{v}_i \leftarrow & \mathbf{a}_c & + & c \cdot (\mathbf{v}_i - \langle \mathbf{v}_c \rangle) + \langle \mathbf{v}_c \rangle & \\ \mathbf{v}_j \leftarrow & \mathbf{a}_h & + & h \cdot (\mathbf{v}_j - \langle \mathbf{v}_h \rangle) + \langle \mathbf{v}_h \rangle. & \end{array}$$

Here $\langle \mathbf{v}_c \rangle$ and $\langle \mathbf{v}_h \rangle$ are the center of mass velocities in the C and H slabs, respectively. Within the two slabs, particles receive incremental changes or a "shear" to their velocities. The amount of shear is governed by the imposed momentum flux, $\mathbf{j}_z(\mathbf{p})$

$$\mathbf{a}_c = -\mathbf{j}_z(\mathbf{p})\Delta t / M_c \tag{1}$$

$$\mathbf{a}_h = +\mathbf{j}_z(\mathbf{p})\Delta t / M_h \tag{2}$$

where $M_{\{c,h\}}$ is the total mass of particles within each of the slabs and Δt is the interval between two separate operations.

To simultaneously impose a thermal flux (J_z) between the slabs we use energy conservation constraints,

$$K_c - J_z \Delta t = c^2 (K_c - \frac{1}{2} M_c \langle \mathbf{v}_c \rangle^2) + \frac{1}{2} M_c (\langle \mathbf{v}_c \rangle + \mathbf{a}_c)^2 \quad (3)$$

$$K_h + J_z \Delta t = h^2 (K_h - \frac{1}{2} M_h \langle \mathbf{v}_h \rangle^2) + \frac{1}{2} M_h (\langle \mathbf{v}_h \rangle + \mathbf{a}_h)^2. \quad (4)$$

Simultaneous solution of these quadratic formulae for the scaling coefficients, c and h, will ensure that the simulation samples from the original microcanonical (NVE) ensemble. Here $K_{\{c,h\}}$ is the instantaneous translational kinetic energy of each slab. At each time interval, it is a simple matter to solve for c, h, $\mathbf{a}_c$, and $\mathbf{a}_h$, subject to the imposed momentum flux, $j_z(\mathbf{p})$, and thermal flux, J_z, values. Since the VSS operations do not change the kinetic energy due to orientational degrees of freedom or the potential energy of a system, configurations after the VSS move have exactly the same energy (and linear momentum) as before the move.

As the simulation progresses, the VSS moves are performed on a regular basis, and the system develops a thermal and/or velocity gradient in response to the applied flux. In a bulk material, it is quite simple to use the slope of the temperature or velocity gradients to obtain either the thermal conductivity or shear viscosity.

The VSS-RNEMD approach is versatile in that it may be used to implement thermal and shear transport simultaneously. Perturbations of velocities away from the ideal Maxwell-Boltzmann distributions are minimal, as is thermal anisotropy. This ability to generate simultaneous thermal and shear fluxes has been previously utilized to map out the shear viscosity of SPC/E water over a wide range of temperatures (90 K) with a single 1 ns simulation.[26]

For this work, we are using the VSS-RNEMD method primarily to generate a shear between the ice slab and the liquid phase, while using a weak thermal gradient to maintain the interface at the 225 K target value. This ensures minimal melting of the bulk ice phase and allows us to control the exact temperature of the interface.

2.3 Computational Details

All simulations were performed using OpenMD,[30,31] with a time step of 2 fs and periodic boundary conditions in all three dimensions. Electrostatics were handled using the damped-shifted force

real-space electrostatic kernel.[32] The systems were divided into 100 bins along the z-axis for the VSS-RNEMD moves, which were attempted every 50 fs.

The interfaces were equilibrated for a total of 10 ns at equilibrium conditions before being exposed to either a shear or thermal gradient. This consisted of 5 ns under a constant temperature (NVT) integrator set to 225K followed by 5 ns under a microcanonical integrator. Weak thermal gradients were allowed to develop using the VSS-RNEMD (NVE) integrator using a small thermal flux (-2.0×10^{-6} kcal/mol/Å^2/fs) for a duration of 5 ns to allow the gradient to stabilize. The resulting temperature gradient was $\approx$ 10K over the entire 100 Å box length, which was sufficient to keep the temperature at the interface within $\pm$1 K of the 225K target.

Velocity gradients were then imposed using the VSS-RNEMD (NVE) integrator with a range of momentum fluxes. These gradients were allowed to stabilize for 1 ns before data collection began. Once established, four successive 0.5 ns runs were performed for each shear rate. During these simulations, snapshots of the system were taken every 1 ps, and statistics on the structure and dynamics in each bin were accumulated throughout the simulations. Although there was some small variation in the measured interfacial width between succcessive runs, no indication of bulk melting (or crystallization) was observed.

3 Results and discussion

3.1 Interfacial width

Any order parameter or time correlation function that changes as one crosses an interface from a bulk liquid to a solid can be used to measure the width of the interface. In previous work on the ice/water interface, Haymet *et al.*[13] have utilized structural features (including the density) as well as dynamic properties (including the diffusion constant) to estimate the width of the interfaces for a number of facets of the ice crystals. Because VSS-RNEMD imposes a lateral flow, parameters that depend on translational motion of the molecules (e.g. diffusion) may be artificially skewed by the RNEMD moves. A structural parameter is not influenced by the RNEMD perturbations to the same degree. Here, we have used the local tetrahedral order parameter as described by Kumar[33] and Errington[34] as our principal measure of the interfacial width. A previous study by Bryk and Haymet also used local tetrahedrality as an order parameter for ice/water interfaces.[35]

The local tetrahedral order parameter, $q(z)$, is given by

$$q(z) = \int_0^L \sum_{k=1}^{N} \left(1 - \frac{3}{8} \sum_{i=1}^{3} \sum_{j=i+1}^{4} \left(\cos\psi_{ikj} + \frac{1}{3} \right)^2 \right) \delta(z_k - z) \mathrm{d}z \Big/ N_z \tag{5}$$

where ψ_{ikj} is the angle formed between the oxygen site on central molecule k, and the oxygen sites on two of the four closest molecules, i and j. Molecules i and j are further restricted to lie withing the first peak in the pair distribution function for molecule k (typically < 3.41 Å for water). $N_z = \int \delta(z_k - z)\mathrm{d}z$ is a normalization factor to account for the varying population of molecules within each finite-width bin. The local tetrahedral order parameter has a range of $(0, 1)$, where the larger values of q indicate a larger degree of tetrahedral ordering of the local environment. In perfect ice $\mathrm{I_h}$ structures, the parameter can approach 1 at low temperatures, while in liquid water, the ordering is significantly less tetrahedral, and values of $q(z) \approx 0.75$ are more common.

To estimate the interfacial width, the system was divided into 100 bins along the z-dimension. The q_z function was time-averaged to give yield a tetrahedrality profile of the system. The profile was then fit to a hyperbolic tangent that smoothly links the liquid and solid states,

$$q(z) \approx q_{liq} + \frac{q_{ice} - q_{liq}}{2} \left[\tanh\left(\frac{z-l}{w} \right) - \tanh\left(\frac{z-r}{w} \right) \right] + \beta \left| z - \frac{r+l}{2} \right|. \tag{6}$$

Here q_{liq} and q_{ice} are the local tetrahedral order parameter for the bulk liquid and ice domains, respectively, w is the width of the interface. l and r are the midpoints of the left and right interfaces, respectively. The last term in eq. (6) accounts for the influence that the weak thermal gradient has on the tetrahedrality profile in the liquid region.

In Figures 1 and 2 we see the z-coordinate profiles for tetrahedrality, temperature, and the x-component of the velocity for the basal and prismatic interfaces. The lower panels show the $q(z)$ (black circles) along with the hyperbolic tangent fits (red lines). In the liquid region, the local tetrahedral order parameter, $q(z) \approx 0.75$ while in the crystalline region, $q(z) \approx 0.94$, indicating a more tetrahedral environment. The vertical dotted lines denote the midpoint of the interfaces (r and l in eq. (6)). The weak thermal gradient applied to the systems in order to keep the interface at 225 ± 5K, can be seen in middle panels. The transverse velocity profile is shown in the upper panels. It is clear from the upper panels that water molecules in close proximity to the surface (i.e.

within 10 Å to 15 Å of the interfaces) have transverse velocities quite close to the velocities within the ice block. There is no velocity discontinuity at the interface, which indicates that the shearing of ice/water interfaces occurs in the "stick" or no-slip boundary conditions.

From the fits using eq. (6), we find the interfacial width for the basal and prismatic systems to be 3.2 ± 0.4 Å and 3.6 ± 0.2 Å , respectively, with no applied momentum flux. Over the range of shear rates investigated, $0.6 \pm 0.3\text{ms}^{-1} \rightarrow 5.3 \pm 0.5\text{ms}^{-1}$ for the basal system and $0.9 \pm 0.2\text{ms}^{-1} \rightarrow 4.5 \pm 0.1\text{ms}^{-1}$ for the prismatic, we found no appreciable change in the interface width. The fit values for the interfacial width (w) over all shear rates contained the values reported above within their error bars. Note that the interfacial widths reported here are based on the hyperbolic tangent parameter w in Eq. 6. This is related to, but not identical with, the 10%-90% intefacial widths commonly used in previous studies.[13,35] To estimate the 10%-90% widths, it is a simple matter to scale the widths obtained from the hyperbolic tangent fits to obtain $w_{10-90} = 2.1971 \times w$.[13,35] This results in w_{10-90} values of 7.0 ± 0.9 Å for the basal face, and 7.9 ± 0.4 Å for the prismatic face. These are somewhat smaller than previously reported values.

3.1.1 Orientational Dynamics

The orientational time correlation function,

$$C_2(t) = \langle P_2(\mathbf{u}(0) \cdot \mathbf{u}(t)) \rangle, \tag{7}$$

gives insight into the local dynamic environment around the water molecules. The rate at which the function decays provides information about hindered motions and the timescales for relaxation. In eq. (7), P_2 is the second-order Legendre polynomial, the vector $\mathbf{u}$ is often taken as HOH bisector, although slightly different behavior can be observed when $\mathbf{u}$ is the vector along one of the OH bonds. The angle brackets denote an ensemble average over all water molecules in a given spatial region.

To investigate the dynamic behavior of water at the ice interfaces, we have computed $C_2(z,t)$ for molecules that are present within a particular slab along the z- axis at the initial time. The change in the decay behavior as a function of the z coordinate is another measure of the change of how the local environment changes across the ice/water interface. To compute these correlation

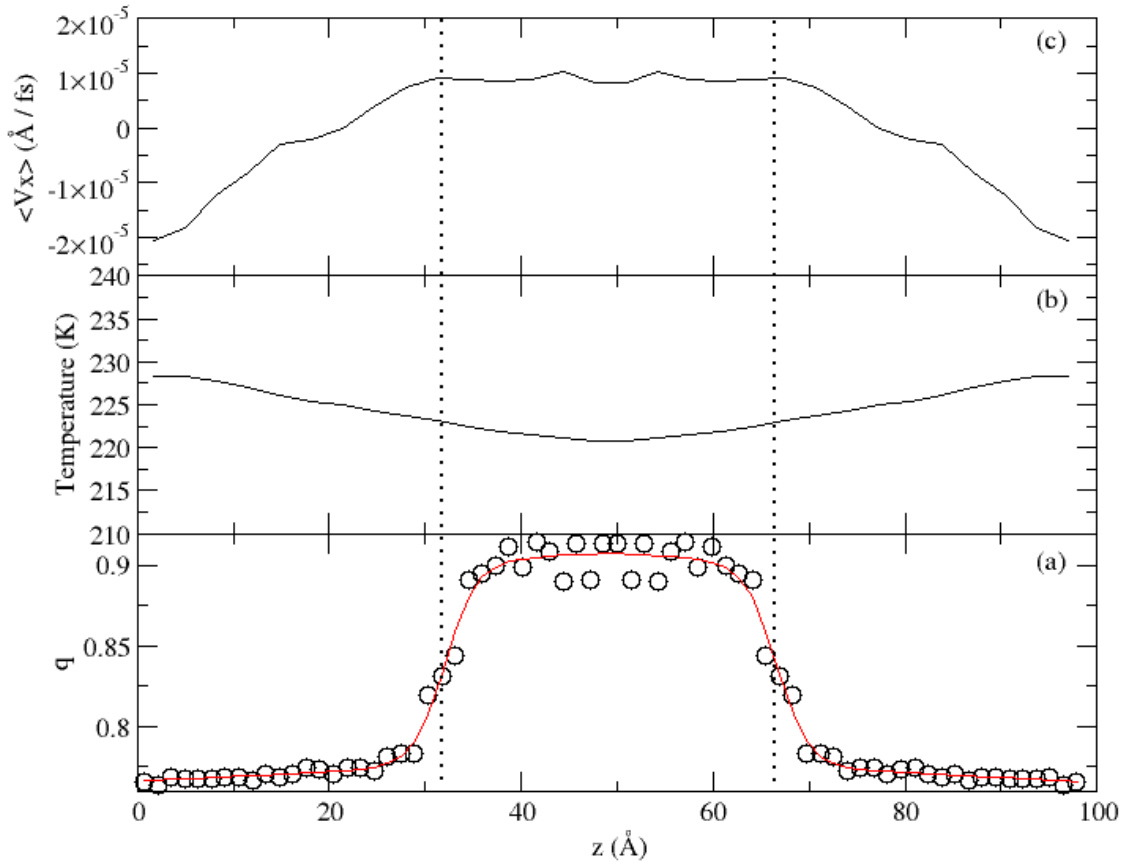

Figure 1: The basal interface with a shear rate of 1.3 ms^{-1}. Lower panel: the local tetrahedral order parameter, $q(z)$, (black circles) and the hyperbolic tangent fit (red line). Middle panel: the imposed thermal gradient required to maintain a fixed interfacial temperature. Upper panel: the transverse velocity gradient that develops in response to an imposed momentum flux. The vertical dotted lines indicate the locations of the midpoints of the two interfaces.

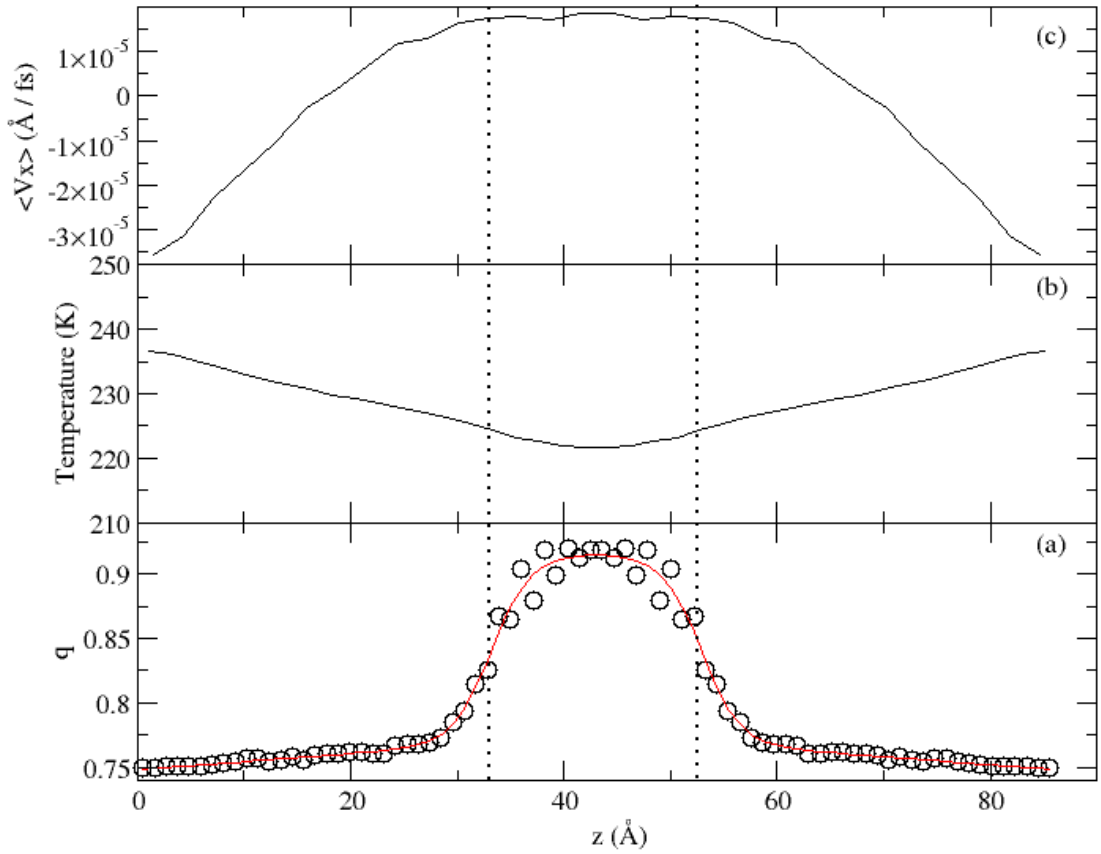

Figure 2: The prismatic interface with a shear rate of 2.0 ms^{-1}. Panel descriptions match those in figure 1

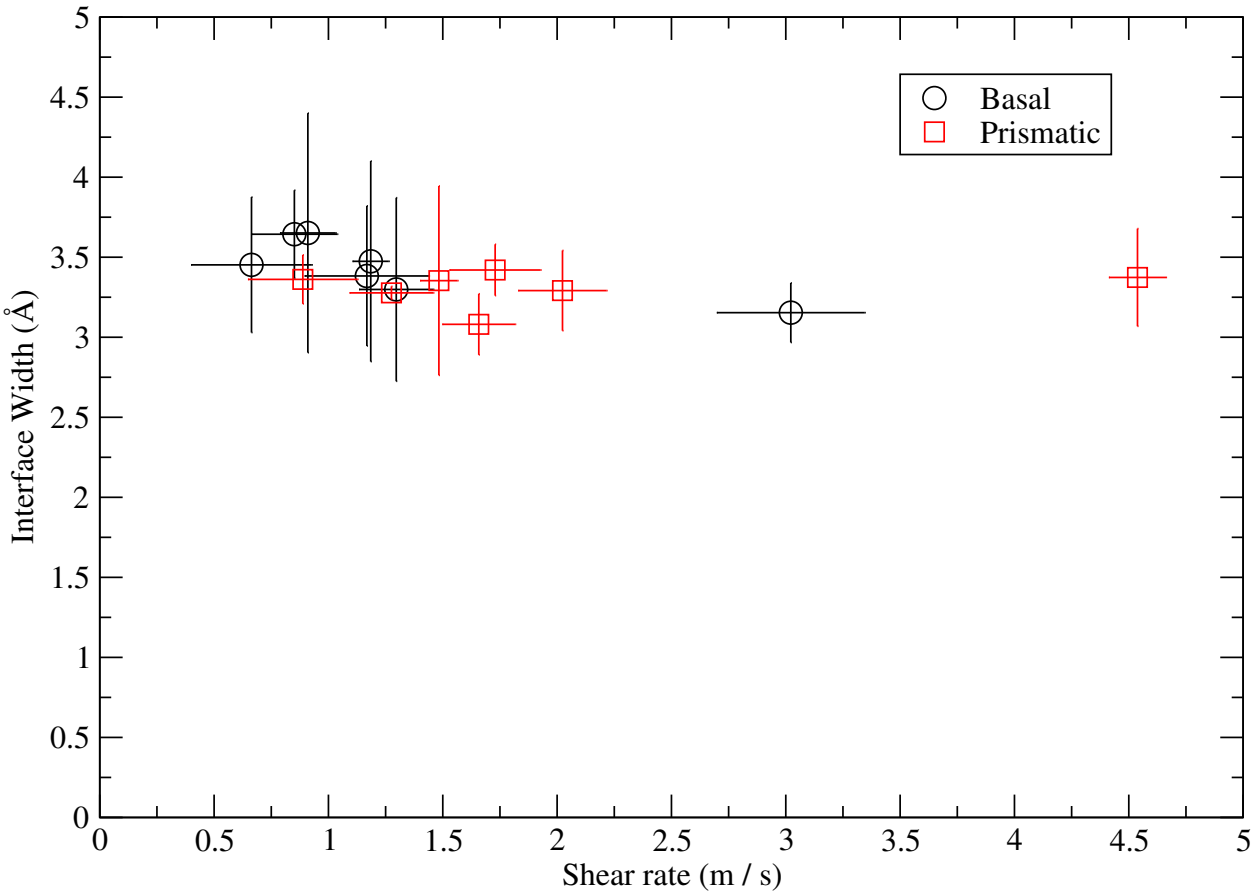

Figure 3: The width of the ice water interfaces (as measured by Eq. 6) exhibits no dependence on the applied shear rate between the ice and water regions.

functions, each of the 0.5 ns simulations was followed by a shorter 200 ps microcanonical (NVE) simulation in which the positions and orientations of every molecule in the system were recorded every 0.1 ps. The systems were then divided into 30 bins along the z-axis and $C_2(t)$ was evaluated for each bin.

In simulations of water at biological interfaces, Furse *et al.* fit $C_2(t)$ functions for water with triexponential functions,[36] where the three components of the decay correspond to a fast (<200 fs) reorientational piece driven by the restoring forces of existing hydrogen bonds, a middle (on the order of several ps) piece describing the large angle jumps that occur during the breaking and formation of new hydrogen bonds,and a slow (on the order of tens of ps) contribution describing the translational motion of the molecules. The model for orientational decay presented recently by Laage and Hynes *et al.*[37,38] also includes three similar decay constants, although two of the time constants are linked, and the resulting decay curve has two parameters governing the dynamics of decay.

In our ice/water interfaces, we are at substantially lower temperatures, and the water molecules are further perturbed by the presence of the ice phase nearby. We have obtained the most reasonable fits using triexponential functions with three distinct time domains, as well as a constant piece to account for the water stuck in the ice phase that does not experience any long-time orientational decay,

$$C_2(t) \approx ae^{-t/\tau_{\text{short}}} + be^{-t/\tau_{\text{middle}}} + ce^{-t/\tau_{\text{long}}} + (1-a-b-c) \tag{8}$$

Average values for the three decay constants (and error estimates) were obtained for each bin. In figures 4 and 5, the three orientational decay times are shown as a function of distance from the center of the ice slab.

Figures 4 and 5 show the three decay constants for the orientational time correlation function for water at varying displacements from the center of the ice slab for both the basal and prismatic interfaces. The vertical dotted lines indicate the locations of the midpoints of the interfaces as determined by the tetrahedrality fits. In the liquid regions, τ_{middle} and τ_{long} have consistent values around 3-4 ps and 20-40 ps, respectively, and increase in value approaching the interface. According to the jump model of Laage and Hynes *et al.*,[37,38] τ_{middle} corresponds to the breaking and making of hydrogen bonds and τ_{long} is explained with translational motion of the molecules (i.e. frame

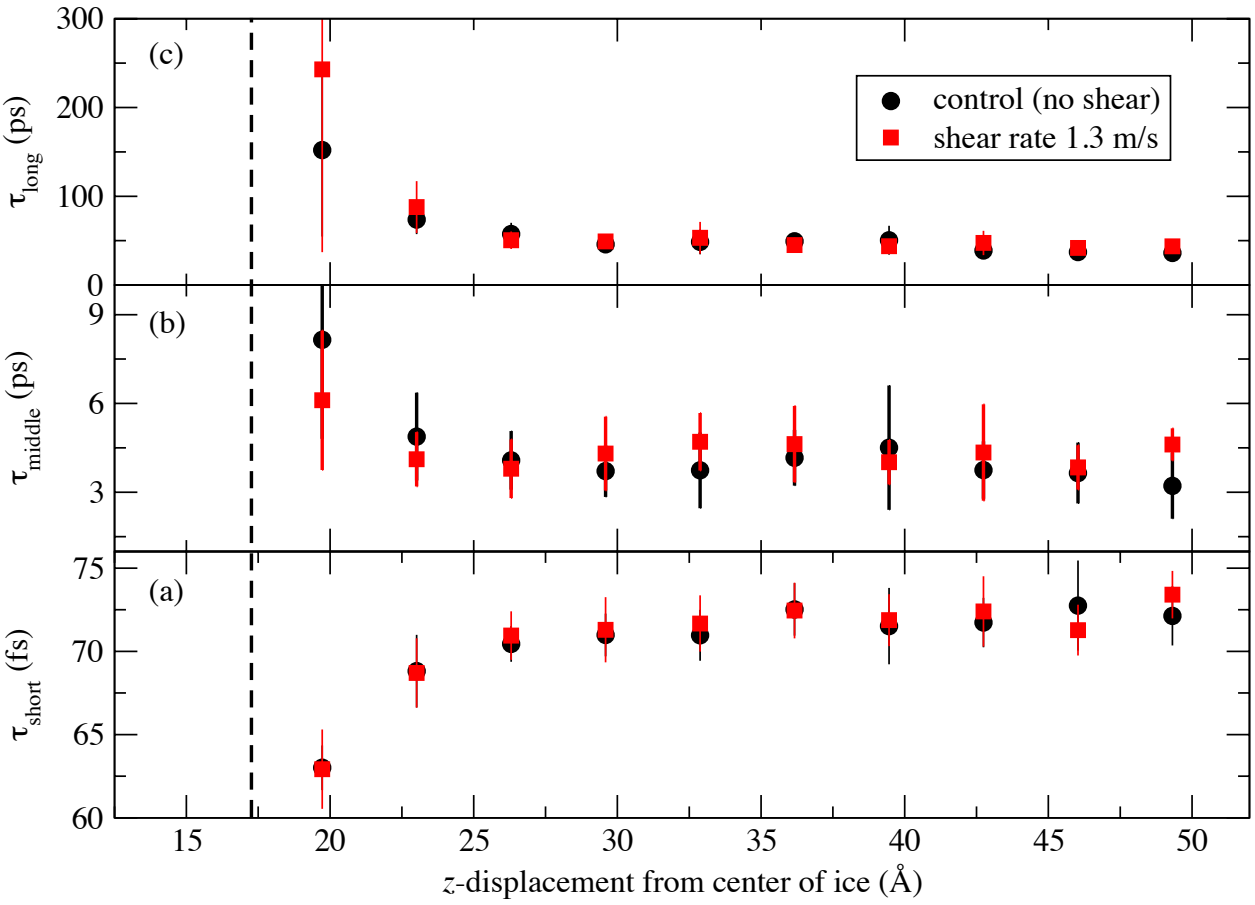

Figure 4: The three decay constants of the orientational time correlation function, $C_2(t)$, for water as a function of distance from the center of the ice slab. The dashed line indicates the location of the basal face (as determined from the tetrahedrality order parameter) and the black and red lines are fits of Eq. 9. The moderate and long time contributions slow down close to the interface which would be expected under reorganizations that involve large motions of the molecules (e.g. frame-reorientations and jumps). The observed speed-up in the short time contribution is surprising, but appears to reflect the restricted motion of librations closer to the interface.

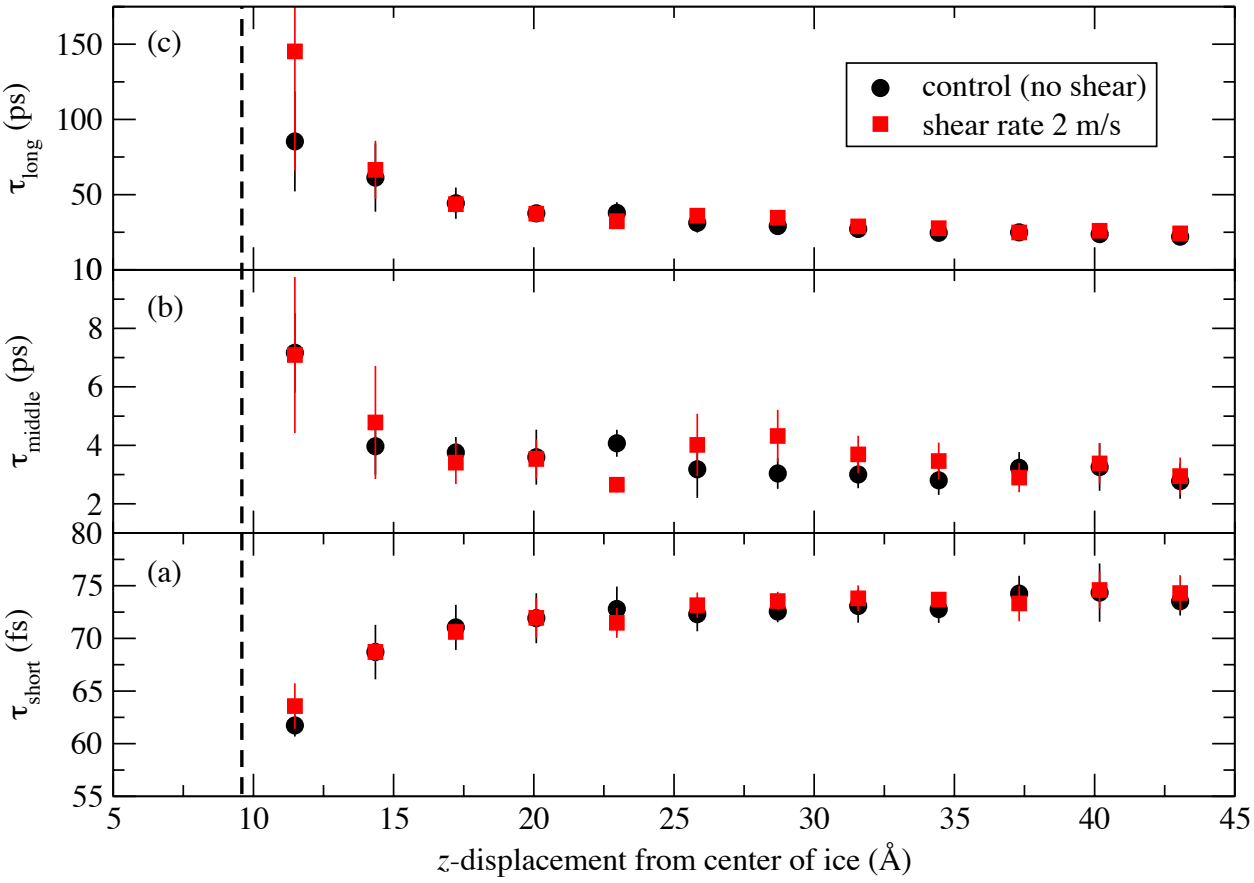

Figure 5: Decay constants for $C_2(t)$ at the prismatic interface. Panel descriptions match those in figure 4.

reorientation). The shortest of the three decay constants, the librational time τ_{short} has a value of about 70 fs in the liquid region, and decreases in value approaching the interface. The observed speed-up in the short time contribution is surprising, but appears to reflect the restricted motion of librations closer to the interface.

The control systems (with no applied momentum flux) are shown with black symbols in figs. 4 and 5, while those obtained while a shear was active are shown in red.

Two notable features deserve clarification. First, there are nearly-constant liquid-state values for τ_{short}, τ_{middle}, and τ_{long} at large displacements from the interface. Second, there appears to be a single distance, d_{basal} or $d_{prismatic}$, from the interface at which all three decay times begin to deviate from their bulk liquid values. To quantify this distance, each of the decay constant z-profiles were fit to

$$\tau(z) \approx \tau_{liquid} + (\tau_{solid} - \tau_{liquid})e^{-(z-z_{wall})/d} \tag{9}$$

where τ_{liquid} and τ_{solid} are the liquid and projected solid values of the decay constants, z_{wall} is the location of the interface, and d is the displacement the deviations occur at (see Figures 4 and 5). The displacements d_{basal} and $d_{prismatic}$ were determined for each of the three decay constants, and then averaged for better statistics. For the basal system, we found d_{basal} for the control set to be 2.9 Å and 2.8 Å for a simulation with a shear rate of 1.3 ms^{-1}. We found $d_{prismatic}$ to be slightly larger than d_{basal} for both the control and an applied shear, with displacements of 3.6 Å for the control system and 3.5 Å for a simulation with a 2 ms^{-1} shear rate. From this we can conclude there is no apparent dependence on the shear rate for the dynamic interface width.

Beaglehole and Wilson have measured the ice/water interface using ellipsometry and find a thickness of approximately 10 Å for both the basal and prismatic faces.[39] Structurally, we have found the basal and prismatic interfacial width to be 3.2 ± 0.4 Å and 3.6 ± 0.2 Å. Decomposition of the spatial dependence of the decay times of $C_2(t)$ shows good agreement with the structural interfacial width determined by the local tetrahedrality.

3.2 Coefficient of Friction of the Interface

As liquid water flows over an ice interface, there is a distance from the structural interface where bulk-like hydrodynamics are recovered. Bocquet and Barrat constructed a theory for the hydrodynamic boundary parameters, which include the slipping length (δ_{wall}) of this boundary layer and the "hydrodynamic position" of the boundary (z_{wall}).[40,41] This last parameter is the location (relative to a solid surface) where the bulk-like behavior is recovered. Work by Mundy *et al.* has helped to combine these parameters into a liquid-solid friction coefficient, which quantifies the resistance to pulling the solid interface through a liquid,[42]

$$\lambda_{\text{wall}} = \frac{\eta}{\delta_{\text{wall}}}. \tag{10}$$

This expression is nearly identical to one provided by Pit *et al.* for the solid-liquid friction of an interface,[43]

$$\lambda = \frac{\eta}{\delta} \tag{11}$$

where δ is the slip length for the liquid measured at the location of the interface itself. In our simulations, the shoulder on the velocity profile indicating the location of the hydrodynamic boundary in the liquid is not always apparent. In some cases, the linear behavior persists nearly up to the interfacial region. For this reason, the hydrodynamic position of the boundary is not always computable, while the Pit approach (Eq. 11) can be used to find the solid-liquid friction coefficient more reliably.

In both the Pit and hydrodynamic boundary expressions, η is the shear viscosity of the bulk-like region of the liquid, a quantity which is easily obtained in VSS-RNEMD simulations by fitting the velocity profile in the region far from the surface.[26] Assuming linear response in the bulk-like region,

$$j_z(p_x) = -\eta \left(\frac{\partial v_x}{\partial z} \right) \tag{12}$$

Substituting this result into eq. (11), we can estimate the solid-liquid coefficient using the slip length,

$$\lambda = -\frac{j_z(p_x)}{\left(\frac{\partial v_x}{\partial z}\right)\delta} \tag{13}$$

For ice / water interfaces, the boundary conditions are no-slip, so projecting the bulk liquid state velocity profile yields a negative slip length. This length is the difference between the structural edge of the ice (determined by the tetrahedrality profile) and the location where the projected velocity of the bulk liquid intersects the solid phase velocity (see Figure 6). The coefficients of friction for the basal and the prismatic facets were determined for shearing along both the x and y axes. The values are given in table 3.

Note that the measured friction coefficient for the basal face is twice that of the prismatic face (regardless of drag direction). These results may seem surprising as the basalface appears smoother than the prismatic with only small undulations of the oxygen positions, while the prismatic surface has deep corrugated channels along the x direction in the crystal system used in this work. However, the corrugations are relatively thin, and the liquid phase water does not appear to populate the channels. The prismatic face therefore effectively presents stripes of solid-phase molecules (making up approximately half of the exposed surface area) with nearly empty space between them. The interfacial friction appears to be independent of the drag direction, so flow parallel to these channels does not explain the lower friction of the prismatic face. A more likely explanation is that the effective contact between the liquid phase and the prismatic face is reduced by the empty corrugations.

Table 3: Solid-liquid friction coefficients (measured in amu fs^{-1})

	Drag direction	
Interface	x	y
basal	0.08 ± 0.02	0.09 ± 0.03
prismatic	0.037 ± 0.008	0.04 ± 0.01

4 Conclusion

We have simulated the basal and prismatic facets of an SPC/E model of the ice I_h / water interface. Using VSS-RNEMD, the ice was sheared relative to the liquid while simultaneously being exposed to a weak thermal gradient which kept the interface at a stable temperature. Calculation of the local tetrahedrality order parameter has shown an apparent independence of the interfacial width

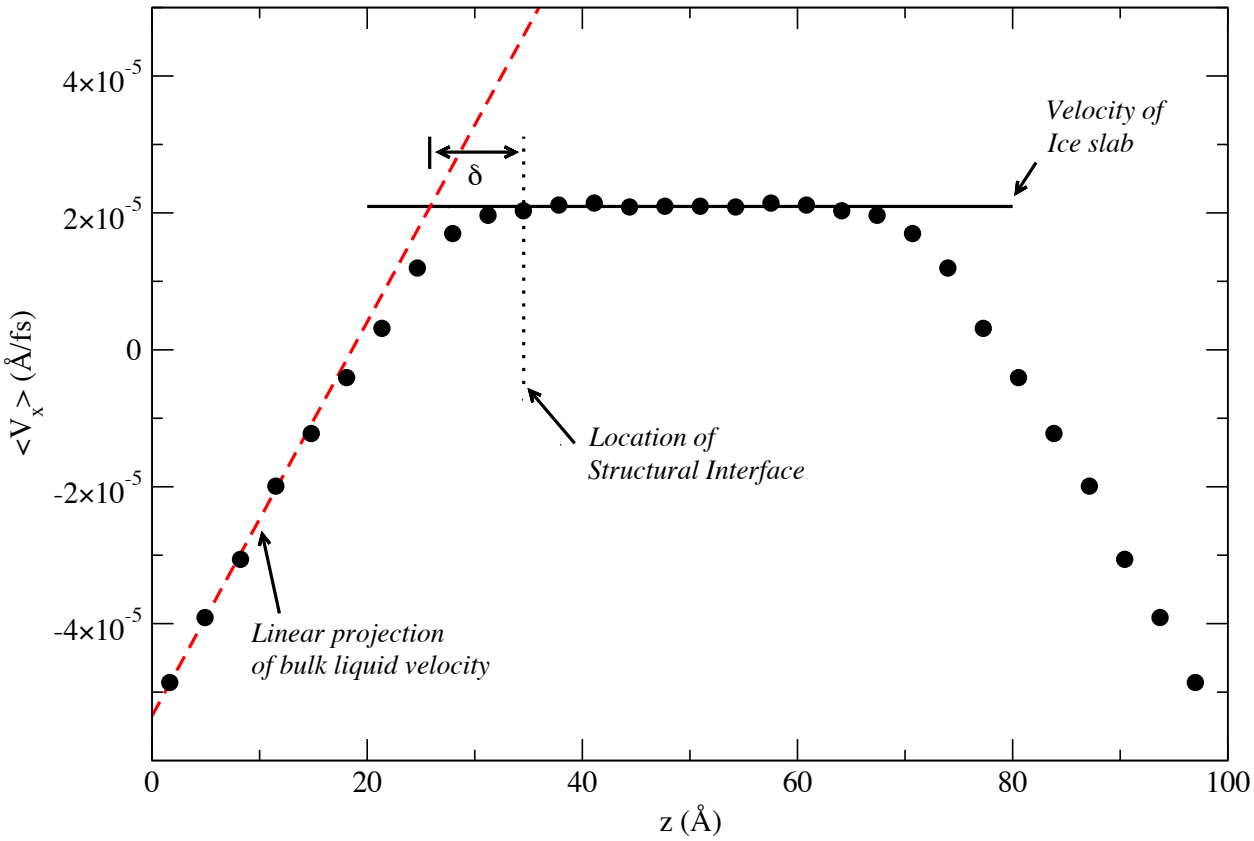

Figure 6: Determining the (negative) slip length (δ) for the ice-water interfaces (which have decidedly non-slip behavior). This length is the difference between the structural edge of the ice (determined by the tetrahedrality profile) and the location where the projected velocity of the bulk liquid (dashed red line) intersects the solid phase velocity (solid black line). The dotted line indicates the location of the ice as determined by the tetrahedrality profile. This example is taken from the basal-face simulation with an applied shear rate of 3.0 ms^{-1}.

on the shear rate. This width was found to be 3.2 ±0.4 Å and 3.6 ±0.2 Å for the basal and prismatic systems, respectively.

Orientational time correlation functions were calculated at varying displacements from the interface, and were found to be similarly independent of the applied momentum flux. The short decay due to the restoring forces of existing hydrogen bonds decreased close to the interface, while the longer-time decay constants increased in close proximity to the interface. There is also an apparent dynamic interface width, d_{basal} and $d_{prismatic}$, at which these deviations from bulk liquid values begin. We found d_{basal} and $d_{prismatic}$ to be approximately 2.8 Å and 3.5 Å . This interfacial width is in good agreement with values determined by the structural analysis of the interface, by the hyperbolic tangent fit of the local tetrahedral order parameter.

The coefficient of liquid-solid friction for each of the facets was also determined. They were found to be 0.07 ± 0.01 amu fs^{-1} and 0.032 ± 0.007 amu fs^{-1} for the basal and prismatic facets respectively. We attribute the large difference between the two friction coefficients to the direction of the shear and to the surface structure of the crystal facets.

5 Acknowledgements

Support for this project was provided by the National Science Foundation under grant CHE-0848243. Computational time was provided by the Center for Research Computing (CRC) at the University of Notre Dame.

References

[1] K. Han and B. N. Hale, *Phys. Rev. B* **45**, 29 (1992).

[2] L. Granasy, *The Journal of Physical Chemistry* **99**, 14182 (1995).

[3] R. R. Vanfleet and J. Mochel, *Surface Science* **341**, 40 (1995).

[4] T. A. Weber and F. H. Stillinger, *The Journal of Physical Chemistry* **87**, 4277 (1983).

[5] H. Sakai, *Surface Science* **348**, 387 (1996).

[6] H. Sakai, *Surface Science* **351**, 285 (1996).

[7] A. Wierzbicki et al., *Biophysical journal* **93**, 1442 (2007).

[8] L. Chapsky and B. Rubinsky, *FEBS letters* **412**, 241 (1997).

[9] J. G. Duman, *Annual Review of Physiology* **63**, 327 (2001), PMID: 11181959.

[10] K. Meister et al., *Proceedings of the National Academy of Sciences* **110**, 1617 (2013).

[11] O. A. Karim, P. A. Kay, and A. D. J. Haymet, *The Journal of Chemical Physics* **92**, 4634 (1990).

[12] S. C. Gay, E. J. Smith, and A. D. J. Haymet, *The Journal of Chemical Physics* **116**, 8876 (2002).

[13] T. Bryk and A. D. J. Haymet, *The Journal of Chemical Physics* **117**, 10258 (2002).

[14] J. A. Hayward and A. D. J. Haymet, *The Journal of Chemical Physics* **114**, 3713 (2001).

[15] J. A. Hayward and A. D. J. Haymet, *Phys. Chem. Chem. Phys.* **4**, 3712 (2002).

[16] O. A. Karim and A. D. J. Haymet, *The Journal of Chemical Physics* **89**, 6889 (1988).

[17] T. Bryk and A. D. J. Haymet, *Journal of Molecular Liquids* **112**, 47 (2004).

[18] E. J. Smith, T. Bryk, and A. D. J. Haymet, *The Journal of Chemical Physics* **123**, 034706 (2005).

[19] P. W. Wilson and A. D. J. Haymet, *The Journal of Physical Chemistry B* **112**, 11750 (2008), PMID: 18720967.

[20] P. W. Wilson and A. D. J. Haymet, *The Journal of Physical Chemistry B* **114**, 12585 (2010).

[21] H. Nada and Y. Furukawa, *Japanese Journal of Applied Physics* **34**, 583 (1995).

[22] H. Nada and Y. Furukawa, *Surface Science* **446**, 1 (2000).

[23] H. Nada and J. P. J. M. van der Eerden, *The Journal of Chemical Physics* **118**, 7401 (2003).

[24] H. Nada and Y. Furukawa, *Polym J* **44**, 690 (2012).

[25] H. Nada and Y. Furukawa, *Journal of Crystal Growth* **283**, 242 (2005).

[26] S. Kuang and J. D. Gezelter, *Molecular Physics* **110**, 691 (2012).

[27] V. Buch, H. Groenzin, I. Li, M. J. Shultz, and E. Tosatti, *Proceedings of the National Academy of Sciences* **105**, 5969 (2008).

[28] T. K. Hirsch and L. Ojamäe, *The Journal of Physical Chemistry B* **108**, 15856 (2004).

[29] H. J. C. Berendsen, J. R. Grigera, and T. P. Straatsma, *The Journal of Physical Chemistry* **91**, 6269 (1987).

[30] M. A. Meineke, C. F. Vardeman, T. Lin, C. J. Fennell, and J. D. Gezelter, *Journal of Computational Chemistry* **26**, 252 (2005).

[31] J. D. Gezelter et al., OpenMD, an Open Source Engine for Molecular Dynamics, Available at `http://openmd.org`.

[32] C. J. Fennell and J. D. Gezelter, *The Journal of Chemical Physics* **124**, 234104 (2006).

[33] P. Kumar, S. V. Buldyrev, and H. E. Stanley, *Proceedings of the National Academy of Sciences* **106**, 22130 (2009).

[34] J. R. Errington and P. G. Debenedetti, *Nature* **409**, 318 (2001).

[35] T. Bryk and A. Haymet, *Molecular Simulation* **30**, 131 (2004).

[36] K. E. Furse and S. A. Corcelli, *Journal of the American Chemical Society* **130**, 13103 (2008), PMID: 18767841.

[37] D. Laage and J. T. Hynes, *The Journal of Physical Chemistry B* **112**, 14230 (2008), PMID: 18942871.

[38] D. Laage, G. Stirnemann, F. Sterpone, R. Rey, and J. T. Hynes, *Annual Review of Physical Chemistry* **62**, 395 (2011), PMID: 21219140.

[39] D. Beaglehole and P. Wilson, *The Journal of Physical Chemistry* **97**, 11053 (1993).

[40] L. Bocquet and J.-L. Barrat, *Phys. Rev. Lett.* **70**, 2726 (1993).

[41] L. Bocquet and J.-L. Barrat, *Phys. Rev. E* **49**, 3079 (1994).

[42] C. J. Mundy, S. Balasubramanian, and M. L. Klein, *Physica A: Statistical Mechanics and its Applications* **240**, 305 (1997).

[43] R. Pit, H. Hervet, and L. Léger, *Tribology Letters* **7**, 147 (1999).